

# Conformational Features and Recognition Properties of a Conformationally Blocked Calix[7]arene Derivative

Carmine Gaeta,<sup>\*,[a]</sup> Carmen Talotta,<sup>[a]</sup> Francesco Farina,<sup>[a]</sup> Gaetano Campi,<sup>[b]</sup> Mercedes Camalli,<sup>[b]</sup> and Placido Neri<sup>[a]</sup>

**Abstract:** The shaping of a calix[7]arene macrocycle into cone-like structure **3**, through exhaustive alkylation of doubly bridged calix[7]arene derivative **2** with bulky groups, has been investigated. Conformational details about the structure adopted by calix[7]arene derivative **3** in solution have been obtained by using chemical shift surface maps, as previously reported by our group. Thus, chemical shift contour plots indicated that **3** adopted a cone-

shaped structure in solution analogous to that adopted by the known *p*-*tert*-butylcalix[7]arene heptacarboxylic acid derivative **4**. Interestingly, the X-ray structure of derivative **3** showed a high degree of similarity to the theoretical

structure, which confirmed the validity of the contour plots method. The pre-organized calix[7]arene host **3** showed interesting recognition abilities toward both organic and alkali cations. In fact, an unprecedented *endo*-cavity complexation of linear and branched alkyl ammonium cations with a larger calix[7]arene host was evidenced. A comparable affinity for branched *t*BuNH<sub>3</sub><sup>+</sup> and linear *n*BuNH<sub>3</sub><sup>+</sup> guests was observed.

**Keywords:** calixarenes • conformational analysis • host–guest systems • molecular recognition • structure elucidation

## Introduction

Recent advances in macrocyclic chemistry have made it possible to develop highly preorganized receptors able to recognize specific guests. In this regard, calix[*n*]arene<sup>[1]</sup> macrocycles have become one of the leading host systems and are currently the most studied receptors in the context of molecular recognition.<sup>[2]</sup> The main reason for this success, apart from their ready availability, is their easy chemical modification,<sup>[3]</sup> which allows the generation of new related systems with improved or profoundly different supramolecular properties. Thus, several calixarene hosts have been reported that showed interesting recognition abilities toward electro-neutral<sup>[4]</sup> and charged anionic<sup>[5]</sup> or cationic<sup>[6]</sup> guests.

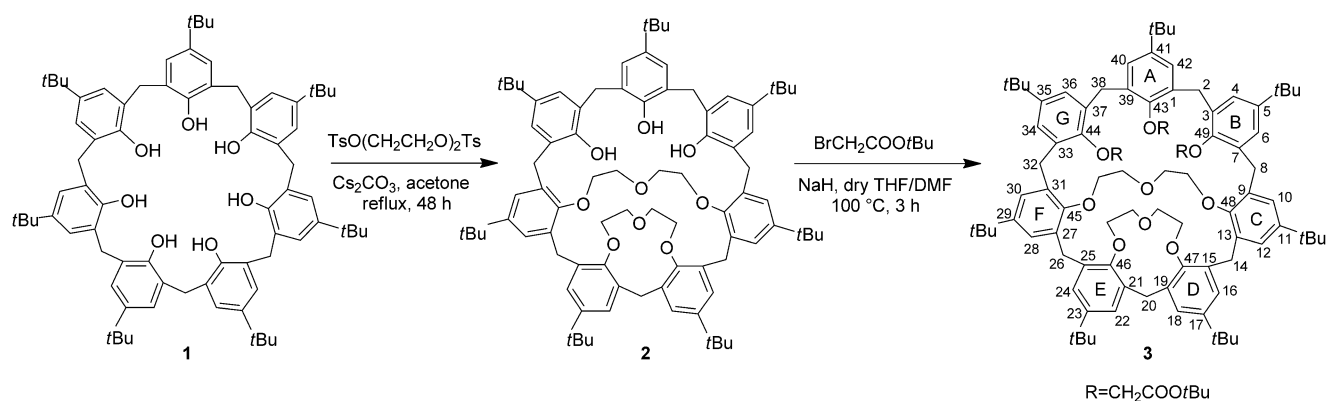
The large majority of these studies have been conducted on the even-membered “major” calix[*n*]arenes (*n* = 4, 6, 8),<sup>[1]</sup> whereas the odd-membered “minor” calix[7]arene<sup>[7]</sup> macrocycle has been scarcely studied. In fact, concerning chemical modification, we reported a procedure to achieve the 1,2,4,6-tetra-*O*-substitution of *p*-*tert*-butylcalix[7]arene **1** (Scheme 1) with high selectivity.<sup>[8]</sup> Successively, the first ex-

amples of 1,4-singly<sup>[9]</sup> and 1,4:2,3-doubly<sup>[10]</sup> bridged calix[7]-arenes were obtained in yields of up to 72 and 76 %, respectively. More recently, examples of monosubstituted,<sup>[11]</sup> singly diacetylamido-bridged,<sup>[11]</sup> and multiply diphosphate-bridged<sup>[12]</sup> calix[7]arenes were reported by Chen and co-workers. Regarding the supramolecular properties of the calix[7]arene macrocycle, our group has reported on the binding ability of a water-soluble *p*-sulfonatocalix[7]arene<sup>[13]</sup> derivative toward organic quaternary ammonium cations. Successively, molecular capsules based on *p*-sulfonatocalix[7]arene and a dicationic Diquat guest have been obtained in the solid state.<sup>[14]</sup>

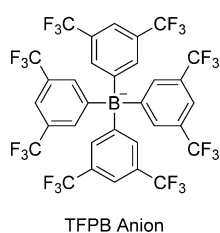
Very recently,<sup>[15]</sup> we have reported on the *endo*-cavity complexation of large calix[6,7]arene derivatives with alkylammonium cations coupled to the weakly coordinating tetrakis[3,5-bis(trifluoromethyl)phenyl]borate (TFPB) anion.<sup>[16]</sup> In particular, we showed that no hint of complexation of [*n*-butylammonium][TFPB] was observed for scarcely preorganized calix[7]arene derivatives. To overcome this kind of problem, we decided to resort to intramolecular bridging as a very convenient method to shape and preorganize larger calixarene macrocycles.<sup>[17,18]</sup> Thus, we focused our attention on doubly bridged calix[7]arene derivatives,<sup>[10]</sup> such as **2** (Scheme 1), in which the presence of two short bridges at the 1,4- and 2,3-positions led to a high level of preorganization and suggested potential applications as molecular hosts in supramolecular chemistry. The 1,4-bridging gives rise to two different tetra- and trimeric subunits in **2** defined by the four alkylated and the three unalkylated phenol rings, respectively. Naturally, the presence of unalkylated OH groups at the lower rim of the trimeric subunit of **2** leaves residual mobility due to their *through-the-annulus*

[a] Dr. C. Gaeta, Dr. C. Talotta, Dr. F. Farina, Prof. P. Neri  
Dipartimento di Chimica e Biologia  
Università degli Studi di Salerno, Via Ponte don Melillo  
84084 Fisciano (Italy)  
Fax: (+39)0899-696-03  
E-mail: cgaeta@unisa.it

[b] Dr. G. Campi, Dr. M. Camalli  
Istituto di Cristallografia, CNR  
Via Salaria Km 29.300  
00015 Moterotondo Scalo (Italy)



Scheme 1. Synthesis of 1,4:2,3-doubly bridged calix[7]arene derivative **3**. Ts = tosyl.



passage, which could be curtailed by the introduction of sufficiently bulky groups.

Herein, we wish to report the first example of complete rigidification of the calix[7]arene macrocycle and the consequent study of the complexation of cationic guests induced by the presence of the weakly coordinat-

ating<sup>[16]</sup> TFPB counterion.

## Results and Discussion

**Synthesis:** Compound **2** was obtained in good yields by direct alkylation of **1** with di(ethylene glycol) ditosylate by following the procedure previously reported by us (Scheme 1).<sup>[10]</sup> 1D and 2D NMR spectroscopy studies revealed that **2** adopted an *all-syn* conformation, similar to the *double-cone pinched* conformation of **1**,<sup>[10,19]</sup> which was characterized by a *syn* combination of the tetra- (cone-like) and trimeric (3/4-cone-like) subunits (see Figure 1).

The presence of two short bridges at the 1,4- and 2,3-positions of the tetrameric cone-like subcavity leads to its rigidification, while variable-temperature (VT) <sup>1</sup>H NMR studies confirmed the expected residual conformational mobility of the trimeric 3/4-cone-like subcavity.<sup>[10]</sup> Interestingly, with respect to the original 28-membered ring of parent **1**, the trimeric 3/4-cone-like sub-ring of **2** is scaled down to a 24-membered ring. In similar previous work,<sup>[20]</sup> it was shown that the conformational rigidification of a 23-membered sub-ring of a 1,5-tetramethylene-bridged calix[8]arene derivative was possible by curtailing the *oxygen-through-the-anulus* route when sufficiently bulky groups were appended at the lower rim of the calix[8]arene macrocycle.

In a similar way, we have now attempted the rigidification of the trimeric 3/4-cone-like subunit of **2** by the introduction of bulky *tert*-butoxycarbonylmethyl groups at the OH functionalities. Exhaustive alkylation of **2** occurred smoothly by using a large excess of *tert*-butylbromoacetate (Scheme 1)

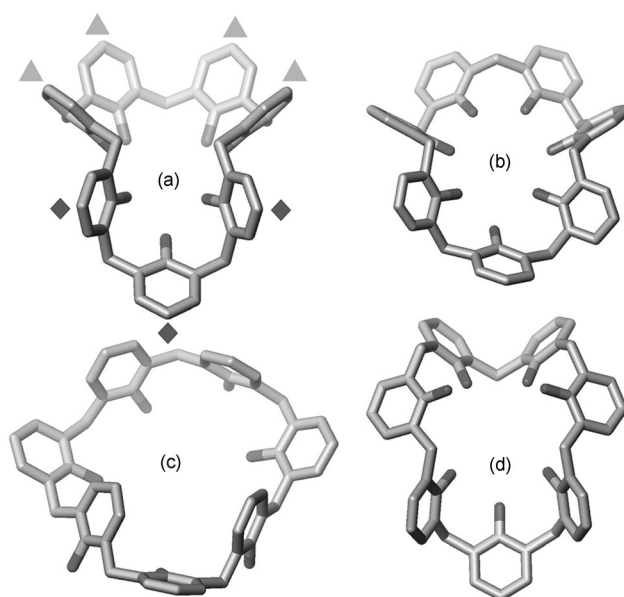


Figure 1. The most common X-ray structures presently found for the calix[7]arene macrocycle: a) X-ray crystal structure of **1** defined as *double-cone pinched* conformation;<sup>[22a]</sup> *p-tert*-butyl groups and hydrogen atoms are omitted for clarity. ▲ and ◆: The calix[7]arene phenol rings forming the tetra- (cone-like) and trimeric (3/4-cone-like) subcavities, respectively. b) X-ray crystal structure of *p*-ethylcalix[7]arene defined as a *pleated-loop/cone* conformation;<sup>[22b]</sup> *p*-ethyl groups and hydrogen atoms are omitted for clarity. c) X-ray crystal structure of *p-tert*-butylcalix[7]arene-heptacarboxylic acid derivative **4**.<sup>[22c]</sup> *p-tert*-butyl and carboxy groups and hydrogen atoms are omitted for clarity. d) X-ray crystal structure of the complex formed by *p*-benzylcalix[7]arene with a uranyl cation in presence of 1,4-diazabicyclo[2.2.2]octane (DABCO) (H atoms, uranyl and HDABCO<sup>+</sup> cations, and solvent molecules are omitted for clarity).<sup>[22d]</sup>

and NaH as a base in a mixture of dry THF/DMF (5:1, v/v) as the solvent at 100 °C for 3 h. After standard workup, product **3** was isolated by column chromatography. The structure of **3** was assigned by means of spectral analysis. In particular, the presence of a pseudomolecular ion signal at *m/z* 1617 in the ESI<sup>+</sup> mass spectrum confirmed the molecular formula. <sup>1</sup>H and <sup>13</sup>C NMR spectra of **3** in CDCl<sub>3</sub> showed the presence of a symmetry plane bisecting one aromatic ring and the opposite ArCH<sub>2</sub>Ar group (Ar–CH<sub>2</sub> symmetry).

Thus, six *t*Bu singlets were present in the  $^1\text{H}$  NMR spectrum ( $\text{CDCl}_3$ , 400 MHz, 298 K) at  $\delta=0.70$ , 1.07, 1.32, 1.34, 1.48, and 1.57 ppm (2:2:2:1:2:1 ratio), while the  $\text{ArCH}_2\text{Ar}$  groups gave rise to four sharp AX systems at  $\delta=3.44/3.51$  ( $J=15.1$  Hz), 3.89/4.22 ( $J=17.2$  Hz), 4.60/4.63 ( $J=15.2$  Hz), and 3.34/5.07 ppm ( $J=13.1$  Hz). The  $^{13}\text{C}$  NMR spectrum displayed four signals at  $\delta=28.1$ , 29.9, 30.2, and 30.8 ppm relative to methylene carbon atoms, while two characteristic resonances (2:1 ratio) relative to the two carbonyl groups were present at  $\delta=168.4$  and 168.0 ppm.

VT NMR studies (400 MHz, TCDE) indicated high conformational stability of **3** and, in particular, with respect to the trimeric 3/4-cone-like subcavity. In fact, no hint of coalescence was observed in the VT  $^1\text{H}$  NMR spectra upon heating to 400 K. This conformational stability was confirmed by prolonged heating in toluene at reflux (up to 4 d), which showed no change in the  $^1\text{H}$  NMR spectrum of **3**. This result proves that the *tert-butyl-through-the-annulus* passage is inhibited in **3** as a result of the small dimension of the trimeric (3/4-cone-like) subcavity and that the *tert-butoxycarbonylmethoxy* substituent is bulky enough to prevent the *oxygen-through-the-annulus* route.

**Definition of the conformation of 3 through theoretically computed  $^1\text{H}$   $\Delta\delta$  and  $^{13}\text{C}$  chemical shift surfaces:** The conformational features of the larger calix[*n*]arenes ( $n=6-8$ )<sup>[21]</sup> become increasingly more complex with the increasing number, *n*, of aryl rings. In fact, an exponentially increasing number of conformations become possible through the increased number of possible combinations of the *syn/anti* dispositions of the aryl rings, joined to their possible inward/outward orientations. Thus, eight extreme conformations are possible for a calix[7]arene macrocycle if a simple “up” or “down” orientation of phenol rings is assumed, but the number is higher if the “out”, “inward”, and “outward” inclinations of the phenol rings are also considered.<sup>[7]</sup> To confirm the high conformational complexity of the calix[7]arene macrocycle, to date, eight different solid-state structures have been determined by X-ray crystallography. The corresponding most common conformations of calix[7]arene skeleton are reported in Figure 1.<sup>[22]</sup>

Naturally, in the case of derivative **3**, the presence of two short bridges at the lower rim requires *syn* orientation between aryl rings E and D and a *syn/outward* geometry between rings F and C (Scheme 1). Both conformational requirements are compatible with each of the conformations reported in Figure 1. Therefore, to shed light on the conformational preferences of **3**, we decided to resort to a proposed novel method for the assessment of calixarene conformations based on the QM GIAO calculation of  $^{13}\text{C}$  and  $^1\text{H}$  NMR chemical shift values of  $\text{ArCH}_2\text{Ar}$  groups.<sup>[23]</sup> In particular, following the reported indications, we used the published chemical shift surface maps<sup>[23b]</sup> in which the  $^1\text{H}$   $\Delta\delta$  (Figure 2a) and  $^{13}\text{C}$   $\delta$  (Figure 2b) values of the calixarene  $\text{ArCH}_2\text{Ar}$  groups are correlated with the  $\phi$  and  $\chi$  torsion angles of the  $\text{Ar}-\text{CH}_2-\text{Ar}$  bonds. Thus, simultaneous fitting of experimental  $^1\text{H}$   $\Delta\delta$  and  $^{13}\text{C}$   $\delta$  values obtained by super-

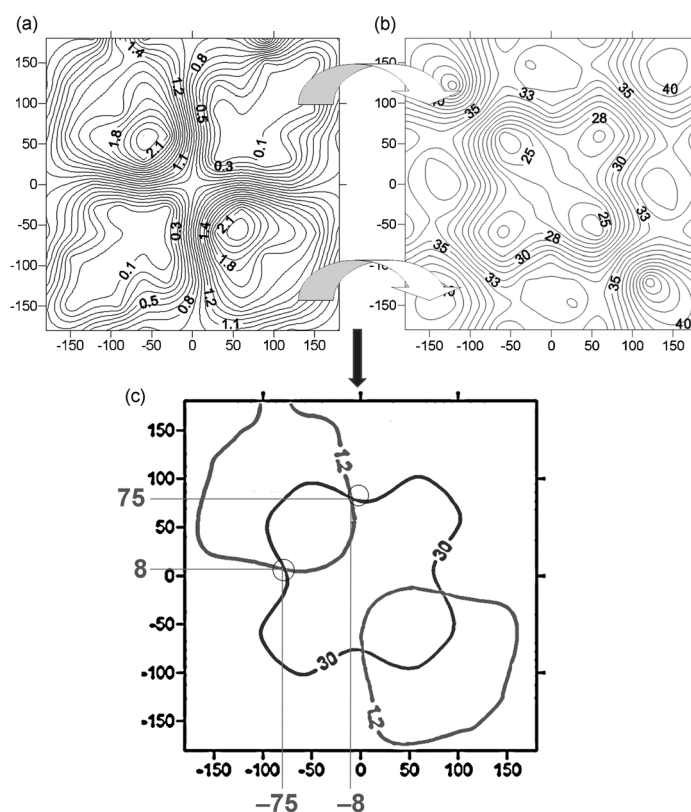


Figure 2. Contour plot representations of the  $^1\text{H}$   $\Delta\delta$  (a) and  $^{13}\text{C}$  (b) chemical shift values [ppm] of the  $\text{ArCH}_2\text{Ar}$  group versus the  $\phi$  and  $\chi$  torsion angles [°].<sup>[23]</sup> c) Computer-assisted graphical superimposition of the lines relative to experimental  $^1\text{H}$   $\Delta\delta=1.2$  ppm and  $^{13}\text{C}$   $\delta=30.0$  ppm values for methylene group 2 (Scheme 1 and Table 1); other lines of the contour plots have been omitted for clarity.

imposition of the relative maps (Figure 2c) allowed us to obtain a series of possible combinations of  $\phi$  and  $\chi$  torsion angles of the  $\text{Ar}-\text{CH}_2-\text{Ar}$  bonds.

To apply this strategy, a complete assignment for both  $^1\text{H}$  and  $^{13}\text{C}$  NMR spectra of **3** was obtained at room temperature by means of a detailed 1D and 2D NMR spectroscopy study (COSY, HSQC, and HMBC 2D spectra, 400 MHz,  $\text{CDCl}_3$ ). Consequently, for each methylene group (2/38, 8/32, 14/26 and 20; see Scheme 1 and Table 1), the simultaneous fitting of the corresponding coupled experimental  $^1\text{H}$   $\Delta\delta$  and  $^{13}\text{C}$   $\delta$  values (Table 1) in the contour plots (Figure 2) was obtained through computer-assisted graphical superimposition<sup>[24]</sup> (see Figure 2c) of the relative  $^1\text{H}$   $\Delta\delta$  and  $^{13}\text{C}$   $\delta$  lines. As an example, Figure 2 illustrates the case of the methylene group at position 2/38:  $^1\text{H}$   $\Delta\delta=1.2$  ppm and  $^{13}\text{C}$   $\delta=30.0$  ppm. Thus, through the coordinates of each intersection point, we obtained  $\phi$  and  $\chi$  torsion angles values of  $+75/-8$  and  $-75/+8^\circ$ . By repeating this procedure for the remaining positions, we obtained the  $\phi$  and  $\chi$  torsion angle values reported in Table 1. These data were then used in a modeling program (Maestro 4.1) to build the possible conformers starting with an open-chain calix[7]arene skeleton.

The first, obvious criterion followed to select compatible conformers was to discard those arrangements that lacked

Table 1.  $\phi$  and  $\chi$  torsion angles derived by fitting of the experimental  $\Delta\delta$   $^1\text{H}$  [a] and  $^{13}\text{C}$  [a]  $\delta$  values for the methylene groups of **3** on the corresponding chemical shift surface.

Atom number	$\delta(^{13}\text{C})^{\text{[a]}}_{\text{exptl}}$ [ppm]	$\Delta\delta(^1\text{H})^{\text{[a]}}_{\text{exptl}}$ [ppm]	$\phi_{\text{calcd}}$ [°]	$\chi_{\text{calcd}}$ [°]
2 and 38	30.0	1.20	+75 -75	-8 +8
8 and 32	30.8	0.34	+87.5 -87.5	+17.5 -17.5
14 and 26	30.2	1.09	+73 -73	+2 -2
20	28.1	1.73	+75 -75	-25 +25

[a] The complete NMR signal assignment leading to  $\Delta\delta$   $^1\text{H}$  and  $^{13}\text{C}$   $\delta$  values for the methylene groups of **3** was obtained by means of a detailed 1D and 2D NMR spectroscopy study (COSY, HSQC, and HMBC 2D NMR spectra, 400 MHz, 298 K,  $\text{CDCl}_3$ ).  $\Delta\delta$   $^1\text{H}$  values were calculated as the distance on the ppm scale between the two doublets of each AX system of  $\text{ArCH}_2\text{Ar}$  groups of **3**.

closure of the calix[7]arene macrocycle. In this way, only the following sequence of torsion angle values was obtained (Table 1): +75/-8, +17.5/-87.5, +73/+2, +25/-75, -2/-73, +87.5/-17.5, and +8/-75°.

Thus, from this sequence of torsion angle values, crude model **3a** was obtained (Figure 3a), which showed a high degree of similarity (see superimposition in Figure 3c) to the crystal structure of *p*-*tert*-butylcalix[7]arene heptacarboxylic acid<sup>[22d]</sup> derivative **4** reported in Figure 1c. The high

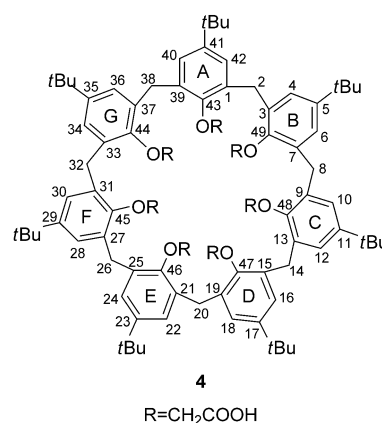


Table 2. Sequence of  $\phi$  and  $\chi$  torsion angles.

Torsion angles <sup>[a]</sup> [°]	<b>3</b> <sup>[b,c]</sup>	<b>3a</b>	<b>3b</b> <sup>[d]</sup>	<b>4</b> <sup>[e,f]</sup>
$\phi$ : C42-C1-C2-C3	+87.9	+75.0	+90.5	+122.5
$\chi$ : C1-C2-C3-C4	-37.1	-8.0	-32.0	-37.7
$\phi$ : C6-C7-C8-C9	+10.8	+17.5	+7.3	+1.4
$\chi$ : C7-C8-C9-C10	-80.6	-87.5	-84.9	-108.6
$\phi$ : C12-C13-C14-C15	+90.7	+73.0	+96.5	+77.2
$\chi$ : C13-C14-C15-C16	-20.3	+2.0	-28.5	-31.3
$\phi$ : C18-C19-C20-C21	+56.3	+25.0	+53.2	+81.2
$\chi$ : C19-C20-C21-C22	-73.1	-75.0	-84.4	-50.1
$\phi$ : C24-C25-C26-C27	+46.3	-2.0	+46.5	+41.0
$\chi$ : C25-C26-C27-C28	-88.9	-73.0	-84.2	-105.6
$\phi$ : C30-C31-C32-C33	+78.8	+87.5	+83.6	+68.0
$\chi$ : C31-C32-C33-C34	+4.0	-17.5	+5.2	+5.0
$\phi$ : C36-C37-C38-C39	+25.0	+8.0	+38.1	+32.7
$\chi$ : C37-C38-C39-C40	-85.5	-75.0	-98.8	-91.1

[a] For the numbering, see Scheme 1. [b] X-ray structure of **3**. [c] The rmsd value with respect to **3a** is 20°. [d] The rmsd value with respect to **3a** is 22°. [e] The rmsd value with respect to **3a** is 29°. [f] The rmsd value with respect to **3** is 17°.

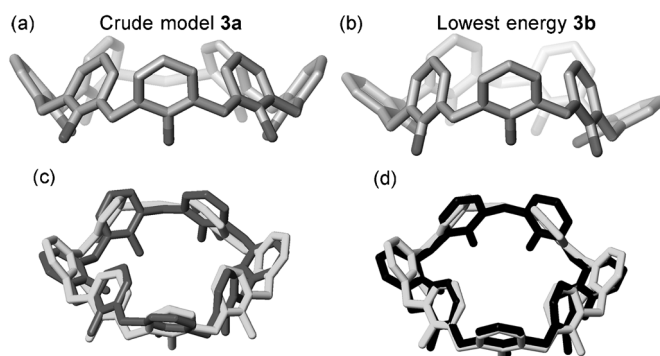


Figure 3. a) Crude model (Maestro 4.1) **3a** obtained by imposing the  $\phi$  and  $\chi$  torsion angle values reported in Table 1 on the calix[7]arene skeleton of **3**. b) Lowest MM3 energy conformation **3b** (MacroModel 9.0,  $\text{CHCl}_3$  GB/SA implicit model solvent) obtained from **3a**. c) Superimposition (rmsd=0.96 Å) of **3a** (light gray) and the X-ray structure (dark gray) of **4**. d) Superimposition (rmsd=0.86 Å) of **3a** (white) and **3b** (black). *tert*-Butyl groups and substituents at the lower rim are omitted for clarity.

degree of similarity between **3a** and **4** was confirmed by a root-mean-square deviation (rmsd) value of 0.96 Å for the superimposition (Figure 3c) and by a rmsd value of 29° for the corresponding torsion angles  $\phi$  and  $\chi$  given in Table 2.

In fact, analogously to **4**, crude-model **3a** displays all calixarene oxygen atoms on the same side of the molecule, with the two bridged F and C rings of tetrameric portion in-

clined outward, while the distal B and G rings of the trimeric subunit are oriented inward. Furthermore, in the calix[7]arene skeleton shown in Figure 3a, the A and B rings (and the equivalent A and G rings) were *syn* oriented in accordance with the experimental  $^{13}\text{C}$   $\delta$  and  $^1\text{H}$   $\Delta\delta$  values of methylene group 2 (Table 1 and Scheme 1).<sup>[25]</sup>

Analogously, a *syn* orientation was found for the couples of adjacent rings C/D (E/F) and D/E. Finally, an *out* orientation was found for crown-3-bridged C and F rings in accordance with an experimental  $^1\text{H}$   $\Delta\delta$  value of 0.34 ppm relative to the pertinent  $\text{ArCH}_2\text{Ar}$  protons in 8.

As previously reported,<sup>[23a]</sup> there is a logical relationship between the canting angle<sup>[26]</sup> of a calixarene aromatic ring and the corresponding  $^1\text{H}$  and  $^{13}\text{C}$  NMR data. In particular, we have deduced that the higher  $^1\text{H}$   $\Delta\delta$  values are predicted for a canting angle,  $\theta$ , ranging from +50 to +100°, corresponding to a cone conformation, with a maximum with regards to a “standing-up” situation for  $\theta = 79^\circ$ . Thus, the high experimental  $^1\text{H}$   $\Delta\delta$  value of 1.73 ppm observed for  $\text{ArCH}_2\text{Ar}$  protons in **20** corresponds to a canting angle of 103 and 86° for the adjacent D and E rings, respectively. In addition, in the theoretical crude-model **3a** (Figure 3a) the

B, D, E, and G rings (Scheme 1) were bent inward toward the calix[7]arene cavity, showing a canting angle of 125, 103, 86, and 120°, respectively, while the A, C, and F rings were oriented outward with a canting angle of 69, 59, and 60°, respectively. Experimentally, an unusually shielded signal at  $\delta = 0.70$  ppm was present in the  $^1\text{H}$  NMR spectrum of **3** ( $\text{CDCl}_3$ , 400 MHz, 298 K) relative to the *t*Bu groups of B and G rings, which was indicative of the self-inclusion of this group inside the calix cavity and suggesting an inward orientation of B and G rings in accordance with **3a**.

Refinement of **3a** was obtained through molecular mechanics calculations (MM3 Force Field,  $\text{CHCl}_3$  GB/SA implicit model solvent).<sup>[27]</sup> The obtained lowest-energy structure, **3b** (Figure 3b), showed only small differences with respect to **3a** (Figure 3a), as demonstrated by a rmsd value of 0.86 Å for the superimposition (Figure 3d) and by a rmsd value of 22° for the corresponding torsion angles  $\phi$  and  $\chi$  given in Table 2.

**Single-crystal X-ray analysis:** Slow crystallization of **3** from a two-component mixture ( $\text{MeOH}/\text{CHCl}_3$ ) afforded colorless crystals, which were suitable for single-crystal X-ray analysis.

Interestingly, derivative **3** adopts a conformation in the solid state (Figure 4) very similar both to that predicted by  $^1\text{H}$  and  $^{13}\text{C}$  chemical shifts surfaces (Figure 3) and to that adopted by *p*-*tert*-butylcalix[7]arene heptacarboxylic acid **4** (Figure 1c); this was confirmed by a rmsd value of 0.6 Å for the superimposition of the X-ray structures of **3** and acid **4** (Figure 5, left).

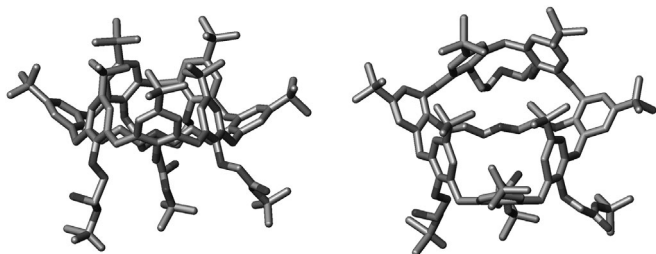


Figure 4. Side view (left) and top view (right) of the X-ray structure of calix[7]arene derivative **3**. Hydrogen atoms are omitted for clarity.

In a similar way, the high degree of similarity between theoretical **3a** (Figure 3a) and the X-ray structure of **3** (Figure 4) was confirmed by a rmsd value of 0.90 Å for their superimposition (Figure 5, right) and by a rmsd value of 20° for the corresponding torsion angles  $\phi$  and  $\chi$  given in Table 2. In analogy to **3a** (Figure 3a), in the X-ray structure of **3** (Figure 4) aromatic rings B, D, E, and G were bent inward towards the calix[7]arene cavity with a canting angle of 103 ( $\Delta\theta = \theta^{\text{crude-model}} - \theta^{\text{X-ray structure}} = 22^\circ$ ), 102 ( $\Delta\theta = 1$ ), 94 ( $\Delta\theta = -8$ ), and 107° ( $\Delta\theta = 13^\circ$ ), respectively. The canting angle values regarding rings A, C, and F, were 62 ( $\Delta\theta = 7^\circ$ ), 35 ( $\Delta\theta = 24$ ), and 36° ( $\Delta\theta = 24^\circ$ ), respectively.

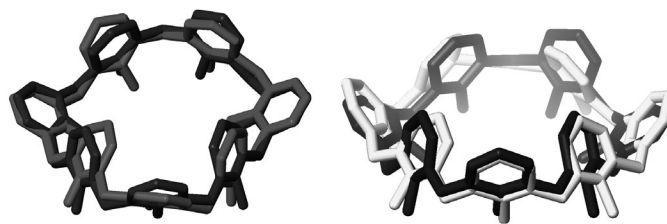


Figure 5. Left: Superimposition (rmsd=0.60 Å) of the X-ray structure (dark gray) of **3** and X-ray structure (light gray) of **4**. Right: Superimposition (rmsd=0.90 Å) of the X-ray structure (black) of **3** and crude model **3a** (white).

As proposed by Ugozzoli and Andreotti,<sup>[28]</sup> an accurate description of larger calixarene conformations can be obtained by means of  $\phi$  and  $\chi$  torsion angle values of  $\text{Ar}-\text{CH}_2-\text{Ar}$  bonds. Thus, when two adjacent aryl rings have a *syn* orientation, the signs of the  $\phi$  and  $\chi$  angles are opposite, whereas they are the same for the *anti* orientation. Examination of the  $\phi$  and  $\chi$  torsion angles reveals that the solid-state conformation of **3** is characterized by the following signs: + −, + −, + −, + −, + −, + +, + −, similar to that of **4** in Figure 1c. The high degree of similarity between the X-ray structures of **3** and **4** was confirmed by a rmsd value of 17° for the corresponding torsion angles  $\phi$  and  $\chi$  given in Table 2.

Interestingly, the solid-state assembly of **3** gives rise to a bilayer-type supramolecular architecture with alternating oxygen-rich polar zones and lipophilic *tert*-butyl regions (Figure 6). In particular, calix[7]arene molecules of **3** are flanked to give a columnar arrangement that runs along the diagonal of the *a,b* plane. Two columns of **3** are stacked on each other through the facing of lipophilic *tert*-butyl regions (Figure 6a). These subunits are stacked along the *c* axis through the facing of lower-rim regions (Figure 6b). Interestingly, inspection of the 2D packing in the *a,b* plane re-

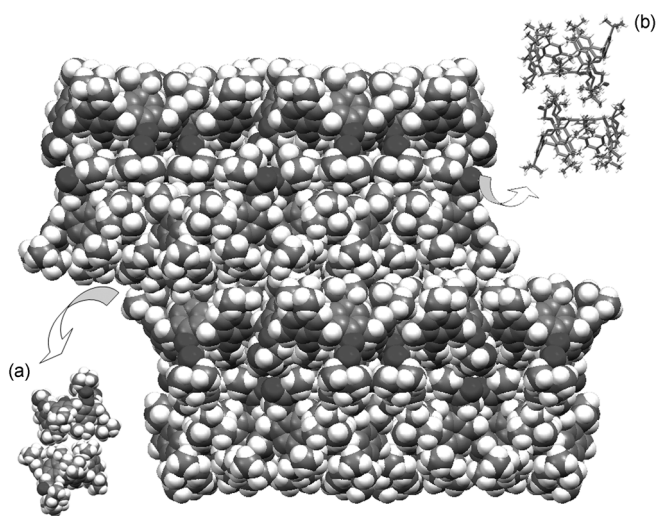


Figure 6. View of the bilayer-type 3D architecture along the diagonal of the *a,b* plane.

vealed that molecules of **3** (Figure 7) fit to form a close-packed arrowhead-motif favored by perfect structural complementarity between the triangular shapes.

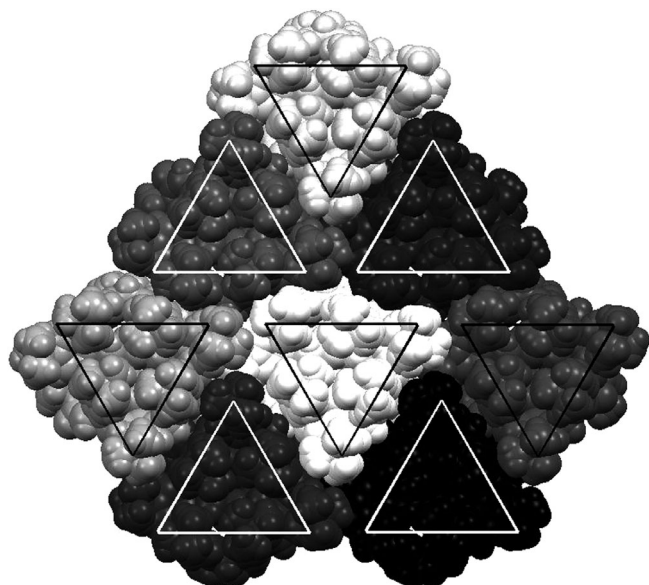


Figure 7. Arrowhead motif derived by the 2D packing of **3** in the *a,b* plane.

#### Binding abilities of **3** toward alkylammonium guests **5a–d**:

<sup>1</sup>H NMR experiments showed interesting recognition properties for calix[7]arene derivative **3** toward [alkylammonium][TFPB] salts **5a–d**. In particular, the addition of the TFPB salt of *n*-butylammonium cation (**5a**) to a solution of **3** in CDCl<sub>3</sub> resulted in significant changes in the <sup>1</sup>H NMR spectrum (Figure 8a). The most evident ones were the appearance of a new set of signals due to the formation of the *n*BuNH<sub>3</sub><sup>+</sup>⊂**3** complex and the presence of *n*-butyl

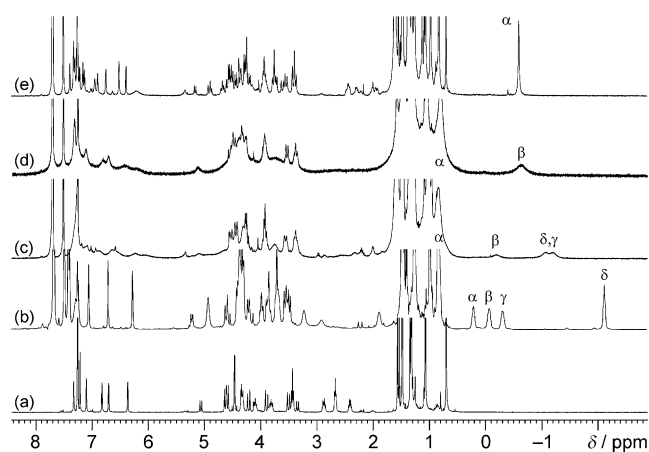
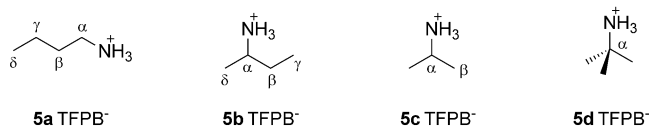


Figure 8. <sup>1</sup>H NMR spectra (CDCl<sub>3</sub>, 400 MHz, 298 K) of a) **3**, b) an equimolar solution (3 mM) of **3** and **5a**, c) an equimolar solution (3 mM) of **3** and **5b**, d) an equimolar solution (3 mM) of **3** and **5c**, and e) an equimolar solution (3 mM) of **3** and **5d**. For definitions of  $\alpha$ ,  $\beta$ ,  $\gamma$ , and  $\delta$ , see structures of **5a–5d**.



resonances in the upfield negative region of the spectrum (Figure 8b).

This latter is a clear indication that **5a** gave *endo*-calix complexation with the alkyl chain shielded by the aromatic rings. Complex formation was also confirmed by an ESI<sup>+</sup> mass spectrum, which gave as the base peak a value of *m/z* 1690, corresponding to supramolecular ion *n*BuNH<sub>3</sub><sup>+</sup>⊂**3**. A COSY-45 spectrum (Figure 9) allowed a complete confident

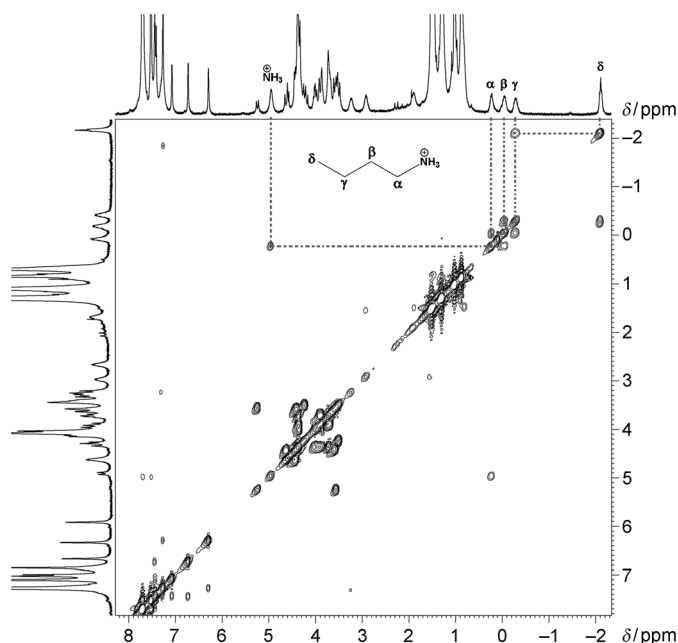


Figure 9. COSY-45 spectrum of an equimolar solution (3 mM) of **3** and **5a**.

assignment of all *n*BuNH<sub>3</sub><sup>+</sup> resonances. Thus, NH<sub>3</sub><sup>+</sup> group at  $\delta = 4.93$  ppm correlates with  $\alpha$  protons at  $\delta = 0.22$  ppm, which in turn is coupled with a  $\beta$  methylene group at  $\delta = -0.05$  ppm, which presents a cross-peak with  $\gamma$  protons at  $\delta = -0.27$  ppm, finally coupled with the  $\delta$  methyl group at  $\delta = -2.11$  ppm (Figure 9). In this way, it is clear that the *n*-butyl protons that experience the highest complexation induced shift (CIS) are those at the  $\delta$  position, which undergo an upfield shift of 4.07 ppm, while the *n*-butyl protons at the  $\alpha$ -,  $\beta$ -, and  $\gamma$ -positions experience CISs of 2.62, 1.40 and 1.52 ppm, respectively. Interestingly, the CIS of the  $\delta$  protons of guest **5a** ( $\Delta\delta = 4.07$  ppm) was significantly higher with respect to that previously observed for analogous protons in *endo*-cavity complexation of an *n*BuNH<sub>3</sub><sup>+</sup> guest with calix[6]arene hosts ( $\Delta\delta = 1.96$  ppm).<sup>[15a]</sup> It is very likely that,

in the  $n\text{BuNH}_3^+\text{C}\mathbf{3}$  complex, the guest is able to penetrate more deeply into the calix[7]arene cavity of  $\mathbf{3}$  and is driven by hydrogen-bond formation between the carbonyl groups at the lower rim of  $\mathbf{3}$  and the ammonium group of guest  $\mathbf{5a}$ . This binding mode was confirmed by the OPLS (optimized potential for liquid simulation) lowest-energy structure of the  $n\text{BuNH}_3^+\text{C}\mathbf{3}$  complex (Figure 10a and b),<sup>[27]</sup> for which it

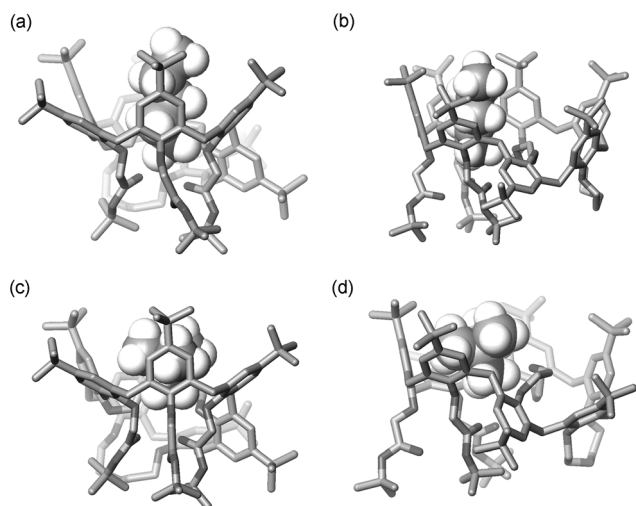


Figure 10. OPLS lowest-energy structures of  $n\text{BuNH}_3^+\text{C}\mathbf{3}$  (a and b) and  $t\text{BuNH}_3^+\text{C}\mathbf{3}$  (c and d) complexes obtained by Monte Carlo conformational searches. Hydrogen atoms of  $\mathbf{3}$  are omitted for clarity.

is possible to observe an *n*-butyl group inside the trimeric 3/4-cone-like subcavity with the ammonium group hydrogen bonded to both etheral oxygen atoms and carbonyl groups. Interestingly, the nitrogen atom sits at a distance of 0.20 Å above the mean plane of the calixarene oxygen atoms of the trimeric 3/4-cone-like subcavity of  $\mathbf{3}$ ; a value that is significantly lower with respect to that previously observed for *endo*-cavity complexation of an  $n\text{BuNH}_3^+$  guest with calix[6]arene hosts (0.76 Å).<sup>[15a]</sup> The apparent association constant for  $n\text{BuNH}_3^+\text{C}\mathbf{3}$  complex was determined by quantitative  $^1\text{H}$  NMR spectroscopy analysis of a 1:1 titration mixture in  $\text{CDCl}_3$ ,<sup>[29]</sup> using toluene as the internal standard, to give a value of  $5.2 \times 10^3 \text{ M}^{-1}$ . It is noteworthy that in  $\text{CDCl}_3$  no trace of complexation of  $n\text{BuNH}_3^+$  guests was observed for  $\mathbf{3}$  in the presence of counterions such as  $\text{Cl}^-$ ,  $\text{PF}_6^-$ , and  $\text{BPh}_4^-$ . This can be ascribed to the sum of two effects, namely, poor solubility and the strong ion-pairing tendency of  $\text{Cl}^-$ ,  $\text{PF}_6^-$ , and  $\text{BPh}_4^-$  salts of  $n\text{BuNH}_3^+$  in  $\text{CDCl}_3$  with respect to the more hydrophobic and weakly coordinating<sup>[16]</sup> TFPB anion. Interestingly, interaction with  $\mathbf{3}$  was also detected for isomeric secondary  $s\text{BuNH}_3^+$   $\mathbf{5b}$  and  $i\text{PrNH}_3^+$   $\mathbf{5c}$  guests. In fact, addition of solid  $[s\text{BuNH}_3][\text{TFPB}^-]$  to a solution of  $\mathbf{3}$  in  $\text{CDCl}_3$  again caused dramatic changes in the  $^1\text{H}$  NMR spectrum (Figure 8c) with the appearance of resonances in the upfield negative region of the spectrum relative to the *s*Bu group of the guest inside the aromatic cavity of  $\mathbf{3}$ . A quantitative  $^1\text{H}$  NMR spectroscopy experiment led to an apparent

association constant for the  $s\text{BuNH}_3^+\text{C}\mathbf{3}$  complex of  $6.2 \times 10^2 \text{ M}^{-1}$ .

Additional interesting *endo*-cavity complexation was obtained with the more cumbersome salt  $\mathbf{5d}$  and  $\mathbf{3}$  (Figure 8e). In fact, in the  $^1\text{H}$  NMR spectrum shown in Figure 8e a singlet shielded at  $\delta = -0.61$  ppm (9H) can be observed that corresponds to the *endo*-cavity disposition of the *t*Bu group. Inspection of the energy-minimized structure of the  $t\text{BuNH}_3^+\text{C}\mathbf{3}$  complex (Figure 10c and d) revealed that the cavity of  $\mathbf{3}$  was large enough to accommodate the bulkier guest  $\mathbf{5d}$ . An apparent association constant for the  $t\text{BuNH}_3^+\text{C}\mathbf{3}$  complex of  $4.8 \times 10^3 \text{ M}^{-1}$  was determined, which was unexpectedly comparable to that of the  $n\text{BuNH}_3^+\text{C}\mathbf{3}$  complex ( $5.30 \times 10^3 \text{ M}^{-1}$ ). In fact, an NMR competition experiment (Figure 11) showed that when  $\mathbf{3}$  was mixed with equimolar

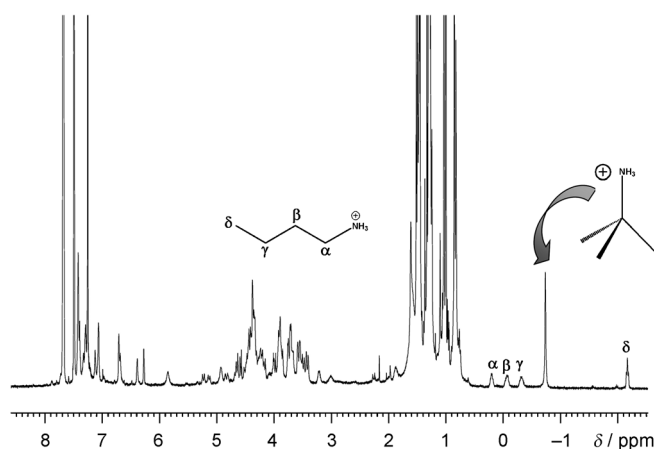


Figure 11.  $^1\text{H}$  NMR spectrum ( $\text{CDCl}_3$ , 400 MHz, 298 K) of an equimolar solution (3 mM) of  $\mathbf{3}$ ,  $\mathbf{5a}$  (3 mM), and  $\mathbf{5d}$  (3 mM).

mixtures of  $[t\text{BuNH}_3][\text{TFPB}]$  and  $[n\text{BuNH}_3][\text{TFPB}]$  salts both  $t\text{BuNH}_3^+\text{C}\mathbf{3}$  and  $n\text{BuNH}_3^+\text{C}\mathbf{3}$  complexes were formed in a 1:1 ratio. Thus, contrary to the results reported by Pappalardo and co-workers<sup>[31]</sup> for smaller *p*-tert-butylcalix[5]arene derivatives, the larger calix[7]arene derivative  $\mathbf{3}$  shows a comparable affinity for isomeric bulky tertiary  $t\text{BuNH}_3^+$  and linear  $n\text{BuNH}_3^+$  guests.

An analogous result was obtained for the complexation of guest  $\mathbf{5c}$ . In fact, the  $^1\text{H}$  NMR spectrum of a 1:1 mixture of the TFPB salt of  $\mathbf{5c}$  and  $\mathbf{3}$  in  $\text{CDCl}_3$  showed a broad signal at  $\delta = -0.62$  ppm characteristic of *endo*-complexation of an isopropyl group shielded by calixarene aromatic rings.  $^1\text{H}$  NMR spectroscopic quantitative analysis of a 1:1 mixture of  $\mathbf{3}$  and  $\mathbf{5d}$  in  $\text{CDCl}_3$  revealed an apparent association constant for the  $i\text{PrNH}_3^+\text{C}\mathbf{3}$  complex of  $3.0 \times 10^3 \text{ M}^{-1}$ . Therefore, compound  $\mathbf{3}$  shows a comparable affinity for linear  $n\text{BuNH}_3^+$  and secondary  $i\text{PrNH}_3^+$  guests. In fact, an NMR competition experiment showed that when  $\mathbf{3}$  was mixed with equimolar mixtures of  $[i\text{PrNH}_3][\text{TFPB}]$  and  $[n\text{BuNH}_3][\text{TFPB}]$  salts both  $n\text{BuNH}_3^+\text{C}\mathbf{3}$  and  $i\text{PrNH}_3^+\text{C}\mathbf{3}$  complexes were formed in a 1:1 ratio.

**Binding ability of **3** toward alkali-metal cations:** Analogously to the alkylammonium guests reported above, calix[7]arene derivative **3** showed interesting complexation properties toward alkali-metal cations. In fact, upon the addition of 0.5 equivalents of solid NaTFPB to a solution of **3** in CDCl<sub>3</sub>, a new set of signals emerged due to the formation of the Na<sup>+</sup>⊂**3** complex (Figure 12a and b). Further addition of cat-

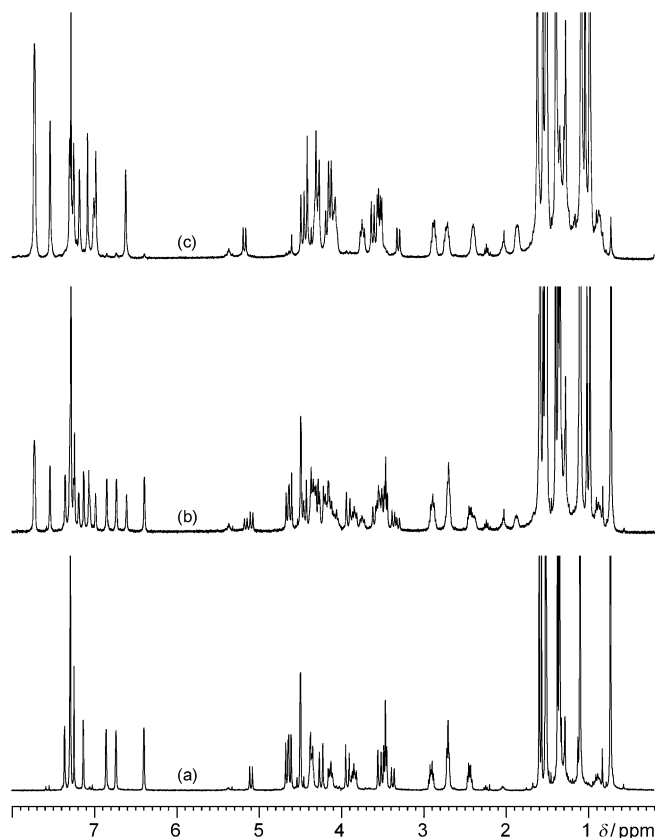


Figure 12. <sup>1</sup>H NMR spectra (CDCl<sub>3</sub>, 400 MHz, 298 K) of a) **3**, b) **3** after the addition of 0.5 equivalents of NaTFPB, and c) **3** after the addition of 1 equivalent of NaTFPB.

ionic guest led to complete complexation (Figure 12c) and a 1:1 stoichiometry was determined by spectral integration. Complete assignment for both <sup>1</sup>H and <sup>13</sup>C NMR spectra of the Na<sup>+</sup>⊂**3** complex in CDCl<sub>3</sub> was obtained at room temperature by means of a detailed 1D and 2D NMR spectroscopy study (2D HSQC and HMBC spectra; 400 MHz, CDCl<sub>3</sub>).

Interestingly, after the addition of NaTFPB to a solution of **3** in CDCl<sub>3</sub>, a downfield shift of the signal of the *t*Bu groups ( $\Delta\delta = 1.13 - 0.70 = 0.43$  ppm) belonging to the B and G aromatic rings was observed. In addition, a downfield shift of aromatic protons ArH<sup>d</sup> (Scheme 1,  $\Delta\delta = 7.17 - 6.70 = 0.47$  ppm) and ArH<sup>e</sup> ( $\Delta\delta = 6.96 - 6.36 = 0.40$  ppm) were also observed. These data indicate that, upon complexation, the B and G rings of **3** switch from the previous inward orientation (Figure 13, left) to the opposite outward orientation (Figure 13, right) with the two *tert*-butoxycarbonylmethoxy groups pointing toward the Na<sup>+</sup> guest.

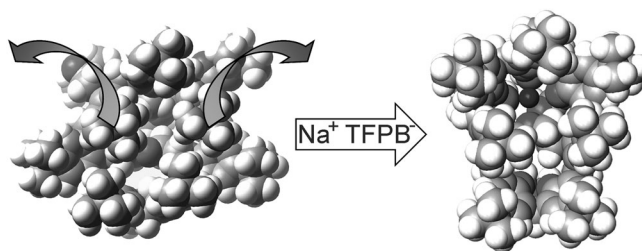


Figure 13. Corey–Pauling–Koltun (CPK) models of the OPLS lowest-energy structures of free host **3** (left) and Na<sup>+</sup>⊂**3** complex (right), as found by Monte Carlo conformational searches.

These adaptive conformational changes were fully confirmed by molecular modeling (Figure 14). In fact, the OPLS lowest-energy structure of Na<sup>+</sup>⊂**3** complex (Figure 14) shows that the cation is encapsulated inside a

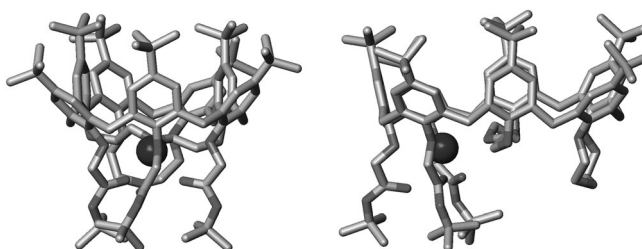


Figure 14. Side views of the computer models of the OPLS lowest-energy structure of the Na<sup>+</sup>⊂**3** complex, as found by Monte Carlo conformational searches.

cavity delimited by the three *tert*-butoxycarbonylmethoxy groups and a crown-3 bridging element (Figures 13 and 14). In particular, inspection of the free (Figure 13 left) and Na<sup>+</sup>-complexed forms (Figure 13 right) revealed that **3** was able to bind the Na<sup>+</sup> guest through an induced-fit mechanism, which originated from the residual conformational flexibility of nonbridged aromatic rings A, B, and G of **3** (see Scheme 1).

An apparent association constant of  $3.4 \times 10^5 \text{ M}^{-1}$  was determined for the Na<sup>+</sup>⊂**3** complex by integration of the slowly exchanging <sup>1</sup>H NMR spectrum of a 1:1 titration mixture in CDCl<sub>3</sub>. It is noteworthy that in CDCl<sub>3</sub> no trace of complexation of the Na<sup>+</sup> guest was observed for **3** in the presence of counterions such as picrate, Cl<sup>-</sup>, PF<sub>6</sub><sup>-</sup>, and BPh<sub>4</sub><sup>-</sup>.

Analogously, the addition of solid KTFPB to a solution of **3** in CDCl<sub>3</sub> caused significant changes in the <sup>1</sup>H NMR spectrum due to the formation of the K<sup>+</sup>⊂**3** complex (Figure 15). Integration of slowly exchanging <sup>1</sup>H NMR signals for both free and complexed calix[7]arene macrocycle **3** lead to an apparent association constant for the K<sup>+</sup>⊂**3** complex of  $3.6 \times 10^3 \text{ M}^{-1}$ . Interestingly, compound **3** displays a selectivity for sodium over potassium of 94 when expressed as the ratio of their association constants.

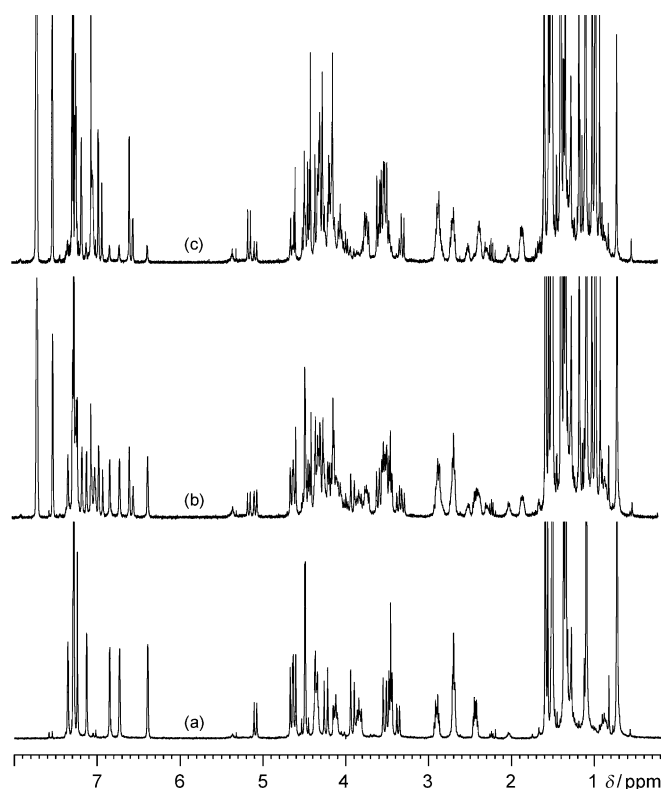


Figure 15.  $^1\text{H}$  NMR spectra ( $\text{CDCl}_3$ , 400 MHz, 298 K) of a) **3**, b) **3** after the addition of 0.5 equivalents of KTFPB, and c) **3** after the addition of 1 equivalent of KTFPB.

## Conclusion

The first example of a completely rigidified calix[7]arene derivative **3** has been synthesized; this showed interesting recognition abilities toward cationic guests. By using previously reported chemical shift surface maps, we predicted that the conformation adopted by **3** was similar to the X-ray structure reported for a the known *p*-*tert*-butylcalix[7]arene heptacarboxylic acid (**4**). This prediction was fully confirmed by single-crystal X-ray analysis of **3**. Interestingly, unprecedented *endo*-cavity complexation by a calix[7]arene host of isomeric linear  $n\text{BuNH}_3^+$  and branched  $s\text{BuNH}_3^+$  and  $t\text{BuNH}_3^+$  cations was observed. Surprisingly, calix[7]arene derivative **3** showed a comparable affinity for branched  $t\text{BuNH}_3^+$  and linear  $n\text{BuNH}_3^+$  guests. In addition, the binding ability of **3** toward alkali-metal cations was also evidenced.

## Experimental Section

**General:** ESI<sup>+</sup>-MS measurements were performed on a Micromass Bio-Q triple quadrupole mass spectrometer equipped with an electrospray ion source, using a mixture of  $\text{H}_2\text{O}/\text{CH}_3\text{CN}$  (1:1) and 5%  $\text{HCOOH}$  as the solvent. Flash chromatography was performed on Merck silica gel (60, 40–63  $\mu\text{m}$ ). All chemicals were of reagent grade and were used without further purification. Anhydrous solvents were purchased from Aldrich. When necessary, compounds were dried in vacuo over  $\text{CaCl}_2$ . Re-

action temperatures were measured externally. Reactions were monitored by TLC on Merck silica gel plates (0.25 mm) and visualized by UV light or by spraying with  $\text{H}_2\text{SO}_4\text{-Ce}(\text{SO}_4)_2$ . Derivatives **1**,<sup>[32]</sup> **2**,<sup>[15]</sup>  $n\text{BuNH}_3^+$  tetrakis[3,5-bis(trifluoromethyl)phenyl]borate,<sup>[15]</sup> and sodium tetrakis[3,5-bis(trifluoromethyl)phenyl]borate<sup>[166]</sup> were synthesized according to literature procedures. NMR spectra were recorded on a Bruker Avance-400 spectrometer (400 ( $^1\text{H}$ ) and 100 MHz ( $^{13}\text{C}$ )); chemical shifts are reported relative to the residual solvent peak ( $\text{CHCl}_3$ :  $\delta = 7.26$  ppm,  $\text{CDCl}_3$ :  $\delta = 77.23$  ppm). Standard pulse programs, provided by the manufacturer, were used for 2D COSY-45, ROESY, HMBC, and HSQC experiments. Monte Carlo conformational searches (10000 steps) were performed with MacroModel-9/Maestro-4.1 program using  $\text{CHCl}_3$  as the solvent (GB/SA model).

**Compound 3:**  $\text{K}_2\text{CO}_3$  (0.88 g, 6.36 mmol) was added, under stirring, to a solution of derivative **2** (0.41 g, 0.32 mmol) in dry  $\text{CH}_3\text{CN}$  (90 mL). The mixture was kept at reflux, under an atmosphere of argon, and after 2 h, *tert*-butylbromoacetate (1.24 g, 0.94 mL, 6.36 mmol) was added. The reaction was stirred at reflux for 12 h under an atmosphere of argon and the solvent was removed under reduced pressure. The residue was dissolved in  $\text{CH}_2\text{Cl}_2$  and washed with  $\text{H}_2\text{O}$  (3  $\times$  50 mL). The organic layer was dried over  $\text{Na}_2\text{SO}_4$ , filtered, and the solvent was removed under reduced pressure. The crude product was subjected to flash chromatography on silica gel using cyclohexane/ethyl acetate (90:10, v/v) as the solvent to give **3** (52%, 0.27 g).  $^1\text{H}$  NMR ( $\text{CDCl}_3$ , 400 MHz, 298 K):  $\delta = 0.70$ , (s, 18H;  $-\text{C}(\text{CH}_3)_3$ ), 1.07 (s, 18H;  $-\text{C}(\text{CH}_3)_3$ ), 1.32 (s, 18H;  $-\text{C}(\text{CH}_3)_3$ ), 1.34 (s, 9H;  $-\text{C}(\text{CH}_3)_3$ ), 1.48 (s, 18H;  $-\text{OC}(\text{CH}_3)_3$ ), 1.57 (s, 9H;  $-\text{OC}(\text{CH}_3)_3$ ), 2.43 (m, 2H;  $-\text{OCH}_2\text{CH}_2\text{OCH}_2\text{CH}_2\text{O}-$ ), 2.67 (t,  $J = 8.0$  Hz, 4H;  $-\text{OCH}_2\text{CH}_2\text{OCH}_2\text{CH}_2\text{O}-$ ), 2.86 (m, 2H;  $-\text{OCH}_2\text{CH}_2\text{OCH}_2\text{CH}_2\text{O}-$ ), 3.34 (AX  $J = 13.2$  Hz, 2H;  $\text{ArCH}_2\text{Ar}$ ), 3.43 (AX,  $J = 15.2$  Hz, 4H;  $\text{ArCH}_2\text{Ar}$ ), 3.44 (brs, 2H;  $-\text{OCH}_2\text{COO}t\text{Bu}$ ), 3.49 (AX,  $J = 13.4$  Hz, 4H;  $\text{ArCH}_2\text{Ar}$ ), 3.80 (m, 2H;  $-\text{OCH}_2\text{CH}_2\text{OCH}_2\text{CH}_2\text{O}-$ ), 3.89 (AX,  $J = 13.6$  Hz, 4H;  $\text{ArCH}_2\text{Ar}$ ), 4.08 (m, 2H;  $-\text{OCH}_2\text{CH}_2\text{OCH}_2\text{CH}_2\text{O}-$ ), 4.23 (AX,  $J = 13.6$  Hz, 4H;  $\text{ArCH}_2\text{Ar}$ ), 4.32 (m, 4H;  $-\text{OCH}_2\text{CH}_2\text{OCH}_2\text{CH}_2\text{O}-$ ), 4.46 (AB,  $J = 15.2$  Hz, 4H;  $-\text{OCH}_2\text{COO}t\text{Bu}$ ), 4.47 (AB,  $J = 15.2$  Hz, 4H;  $-\text{OCH}_2\text{COO}t\text{Bu}$ ), 4.58 (AX,  $J = 13.4$  Hz, 4H;  $\text{ArCH}_2\text{Ar}$ ), 4.62 (AX,  $J = 15.2$  Hz, 4H;  $\text{ArCH}_2\text{Ar}$ ), 5.07 (AX,  $J = 13.2$  Hz, 2H;  $\text{ArCH}_2\text{Ar}$ ), 6.36 (brs, 2H;  $\text{ArH}$ ), 6.70 (brs, 2H;  $\text{ArH}$ ), 6.82 (brs, 2H;  $\text{ArH}$ ), 7.10 (d,  $J = 2.4$  Hz, 2H;  $\text{ArH}$ ), 7.21 (s, 2H;  $\text{ArH}$ ), 7.26 (brs, 2H;  $\text{ArH}$ ), 7.32 ppm (d,  $J = 2.4$  Hz, 2H;  $\text{ArH}$ );  $^{13}\text{C}$  NMR ( $\text{CDCl}_3$ , 100 MHz, 298 K):  $\delta = 28.1$  (t,  $\text{ArCH}_2$ ), 28.3 (q,  $-\text{OCH}_2\text{COOC}(\text{CH}_3)_3$ ), 28.6 (q,  $-\text{OCH}_2\text{COOC}(\text{CH}_3)_3$ ), 29.8 (t,  $\text{ArCH}_2$ ), 30.2 (t,  $\text{ArCH}_2$ ), 30.8 (q,  $-\text{C}(\text{CH}_3)_3$ ), 30.9 (t,  $\text{ArCH}_2$ ), 31.6 (q,  $-\text{C}(\text{CH}_3)_3$ ), 31.7 (q,  $-\text{C}(\text{CH}_3)_3$ ), 31.8 (q,  $-\text{C}(\text{CH}_3)_3$ ), 34.1 (s,  $-\text{C}(\text{CH}_3)_3$ ), 34.4 (s,  $-\text{C}(\text{CH}_3)_3$ , 6C), 67.9 (t,  $-\text{OCH}_2\text{CH}_2\text{OCH}_2\text{CH}_2\text{O}-$ ), 69.2 (t,  $-\text{OCH}_2\text{COOC}(\text{CH}_3)_3$ ), 70.7 (t,  $-\text{OCH}_2\text{COOC}(\text{CH}_3)_3$ ), 71.4 (t,  $-\text{OCH}_2\text{CH}_2\text{OCH}_2\text{CH}_2\text{O}-$ ), 74.0 (t,  $-\text{OCH}_2\text{CH}_2\text{OCH}_2\text{CH}_2\text{O}-$ ), 74.4 (t,  $-\text{OCH}_2\text{CH}_2\text{OCH}_2\text{CH}_2\text{O}-$ ), 81.9 (s,  $-\text{OCH}_2\text{COOC}(\text{CH}_3)_3$ , 3C), 123.3 (d,  $\text{C}_{\text{Ar}}\text{H}$ ), 123.5 (d,  $\text{C}_{\text{Ar}}\text{H}$ ), 124.2 (d,  $\text{C}_{\text{Ar}}\text{H}$ ), 125.8 (d,  $\text{C}_{\text{Ar}}\text{H}$ ), 127.7 (d,  $\text{C}_{\text{Ar}}\text{H}$ ), 127.9 (d,  $\text{C}_{\text{Ar}}\text{H}$ ), 128.4 (d,  $\text{C}_{\text{Ar}}\text{H}$ ), 131.6 (s,  $\text{C}_{\text{Ar}}\text{CH}_2$ ), 132.4 (s,  $\text{C}_{\text{Ar}}\text{CH}_2$ ), 132.8 (s,  $\text{C}_{\text{Ar}}\text{CH}_2$ ), 131.6 (s,  $\text{C}_{\text{Ar}}\text{CH}_2$ ), 133.7 (s,  $\text{C}_{\text{Ar}}\text{CH}_2$ ), 134.2 (s,  $\text{C}_{\text{Ar}}\text{CH}_2$ , 2C), 134.8 (s,  $\text{C}_{\text{Ar}}\text{CH}_2$ ), 146.0 (s,  $\text{C}_{\text{Ar}}\text{C}(\text{CH}_3)_3$ , 4C), 146.4 (s,  $\text{C}_{\text{Ar}}\text{C}(\text{CH}_3)_3$ , 3C), 151.6 (s,  $\text{C}_{\text{Ar}}\text{O}$ , 3C), 152.4 (s,  $\text{C}_{\text{Ar}}\text{O}$ ), 154.7 (s,  $\text{C}_{\text{Ar}}\text{O}$ ), 168.0 (s,  $\text{C}=\text{O}$ ), 168.4 ppm (s,  $\text{C}=\text{O}$ ); ESI<sup>+</sup>-MS:  $m/z$  1617 [ $\text{M}+\text{H}^+$ ]; elemental analysis calcd (%) for  $\text{C}_{103}\text{H}_{140}\text{O}_{15}$ : C 76.45, H 8.72; found: C 76.55, H 8.62.

**X-ray crystallography:** The single-crystal X-ray diffraction measurements were collected on an XCS-Huber four-circle diffractometer (University of Rome "La Sapienza", Department of Chemistry,) using graphite-monochromatized  $\text{MoK}\alpha$  radiation (0.71073 Å). The crystal was sealed with its mother liquid in Lindermann capillaries to avoid efflorescence. The cell parameters were refined by least squares from the angular positions of 50 reflections; the data were measured at room temperature for  $0.85^\circ < 2\theta < 20.81^\circ$  using a  $\theta/2\theta$  scan technique and processed to yield  $I$  and  $\sigma(I)$  values corrected for Lorentz, polarization, and shape anisotropy effects; no decay effect was observed. A total of 5435 independent reflections with  $F_o > 3\sigma(F_o)$  were processed by the direct methods, which provided the complete structure in the  $P2_1/a$  space group. All non-hydrogen atoms were refined by a full-matrix least-squares method with anisotropic thermal parameters, except for three carbon atoms refined with isotropic thermal factors due to disorder that could not be modeled. Due to the low-quality data mentioned, we enhanced the observed reflections/pa-

rameters ratio refinement using constraints by setting the benzene rings as rigid bodies; the final *R* value was 0.10. The hydrogen atoms were included in geometric positions (C–H=0.96 Å) and given thermal parameters equivalent to 1.3 times those of the parent atom and allowed to ride on it. The final difference Fourier map, with a root-mean-square deviation of electron density of 0.06 e<sup>−3</sup> showed minimum and maximum values of −0.47 and 0.44, respectively. Calculations were performed by using the XCS data collection program,<sup>[33]</sup> DARX2002 data reduction program, and “Il milione” structure determination and refinement package.<sup>[34]</sup> Full details are given in Table 3.

Table 3. Data collection parameters for compound 3.

	3
formula	C <sub>103</sub> H <sub>140</sub> O <sub>15</sub>
<i>M<sub>r</sub></i>	1618.26
<i>a</i> [Å]	17.905(4)
<i>b</i> [Å]	23.354(5)
<i>c</i> [Å]	24.111(5)
$\alpha$ [°]	90.00
$\beta$ [°]	97.84(2)
$\gamma$ [°]	90.00
<i>V</i> [Å <sup>3</sup> ]	9988(4)
<i>Z</i>	4
crystal system	monoclinic
$\rho_{\text{calc}}$ [g cm <sup>−3</sup> ]	1.073
<i>F</i> (000)	3496
$\mu$ [mm <sup>−1</sup> ]	0.070
<i>h, k, l</i> min/max	0/17, 0/23, −23/23
resolution range [Å]	1.000–23.886
reflins collected	10302
independent reflins [ <i>R<sub>int</sub></i> ]	6195 [0.070]
parameters refined	754
<i>a, b, c</i> , in the $w = 1.0/a + bF_o + cF_o^2$	0.0084, 1.0000, 0.0039
weighting scheme	
<i>R</i> , <i>wR</i>	0.100, 0.146
goodness of fit, <i>S</i>	0.885
max mean shift/error	0.001/0.000

CCDC-820352 contains the supplementary crystallographic data for this paper. These data can be obtained free of charge from The Cambridge Crystallographic Data Centre via [www.ccdc.cam.ac.uk/data\\_request/cif](http://www.ccdc.cam.ac.uk/data_request/cif).

**General procedure for the synthesis of the ammonium TFPB salts:** A solution of NaTFPB<sup>[16b]</sup> (0.67 mmol) in dry methanol (2 mL) was added to the solution of appropriate (*n*-butyl, *sec*-butyl, or isopropylammonium) chloride salts (0.52 mmol) in dry methanol (3 mL). The resulting solution was stirred overnight. After removing methanol by evaporation, deionized water was added, and the brown solid was filtered off and dried under vacuum for 24–48 h.

[*t*BuNH<sub>3</sub>][TFPB]: <sup>1</sup>H NMR ([D<sub>6</sub>]DMSO, 400 MHz, 298 K):  $\delta$  = 1.21 (s, 9H; (CH<sub>3</sub>)<sub>3</sub>CNH<sub>3</sub><sup>+</sup>), 7.70 ppm (brs, 12H; ArH<sup>TFPB</sup>); <sup>13</sup>C NMR ([D<sub>6</sub>]DMSO, 100 MHz, 298 K):  $\delta$  = 27.0, 51.0, 117.6, 119.9, 122.6, 125.4, 128.1, 128.3, 128.6, 129.0, 134.1, 160.3, 160.7, 161.3, 161.7 ppm.

[*s*BuNH<sub>3</sub>][TFPB]: <sup>1</sup>H NMR ([D<sub>6</sub>]DMSO, 400 MHz, 298 K):  $\delta$  = 0.87 (t, *J* = 7.2 Hz, 3H; CH<sub>3</sub>CH(<sup>+</sup>NH<sub>3</sub>)CH<sub>2</sub>CH<sub>3</sub>), 1.10 (d, *J* = 7.4 Hz, 3H; CH<sub>2</sub>CH(<sup>+</sup>NH<sub>3</sub>)CH<sub>2</sub>CH<sub>3</sub>), 1.43 (m, 2H; CH<sub>3</sub>CH(<sup>+</sup>NH<sub>3</sub>)CH<sub>2</sub>CH<sub>3</sub>), 3.05 (m, 1H; CH<sub>3</sub>CH(<sup>+</sup>NH<sub>3</sub>)CH<sub>2</sub>CH<sub>3</sub>), 7.61 ppm (brs, 12H, ArH<sup>TFPB</sup>); <sup>13</sup>C NMR ([D<sub>6</sub>]DMSO, 100 MHz, 298 K):  $\delta$  = 9.61, 17.6, 27.1, 48.3, 117.6, 121.9, 126.3, 127.9, 128.8, 129.3, 130.6, 134.1, 159.9, 160.7, 161.5, 166.3 ppm;

[*i*PrNH<sub>3</sub>][TFPB]: <sup>1</sup>H NMR (CD<sub>3</sub>OD 400 MHz, 298 K):  $\delta$  = 1.30 (d, *J* = 6.4 Hz, 6H; (CH<sub>3</sub>)<sub>2</sub>CHNH<sub>3</sub><sup>+</sup>), 3.41 (sept, *J* = 6.4 Hz, 1H; (CH<sub>3</sub>)<sub>2</sub>CHNH<sub>3</sub><sup>+</sup>), 7.71 ppm (brs, 12H; ArH<sup>TFPB</sup>); <sup>13</sup>C NMR ([D<sub>6</sub>]DMSO, 100 MHz, 298 K):  $\delta$  = 20.3, 43.1, 117.5, 122.7, 125.4, 128.1, 128.3, 128.6, 134.1, 160.3, 160.8, 161.3, 161.8 ppm.

***n*BuNH<sub>3</sub><sup>+</sup>C3 complex:** Compound 3 (0.002 g, 1.23 × 10<sup>−3</sup> mmol) was dissolved in CDCl<sub>3</sub> (0.4 mL; 3.0 × 10<sup>−3</sup> M solution). Then, a solution of *n*-butylammonium tetrakis[3,5-bis(trifluoromethyl)phenyl]borate salt in CDCl<sub>3</sub> (1.23 × 10<sup>−3</sup> mmol, 6.1 × 10<sup>−3</sup> M) was added and the mixture was stirred for 15 min at room temperature. Then, the solution was transferred to an NMR tube for 1D and 2D NMR spectra acquisition. <sup>1</sup>H NMR (CDCl<sub>3</sub>, 400 MHz, 298 K):  $\delta$  = −2.10 (brs, 3H; (CH<sub>2</sub>)<sub>3</sub>), −0.31 (m, 2H; (CH<sub>2</sub>)<sub>2</sub>), −0.07 (m, 2H, (CH<sub>2</sub>)<sub>β</sub>), 0.21 (m, 2H, (CH<sub>2</sub>)<sub>α</sub>), 0.85 (s, 18H; −C(CH<sub>3</sub>)<sub>3</sub>), 1.00 (s, 18H; −C(CH<sub>3</sub>)<sub>3</sub>), 1.28 (s, 27H; −C(CH<sub>3</sub>)<sub>3</sub>), 1.49 (s, 18H; −OC(CH<sub>3</sub>)<sub>3</sub>), 1.51 (s, 9H; −OC(CH<sub>3</sub>)<sub>3</sub>), 3.50 (AX, *J* = 14.8 Hz, 4H; ArCH<sub>2</sub>Ar), 3.56 (AX, *J* = 12.4 Hz, 2H; ArCH<sub>2</sub>Ar), 3.58 (AX, *J* = 12.8 Hz, 4H; ArCH<sub>2</sub>Ar), 3.68 (brs, 4H; −OCH<sub>2</sub>CH<sub>2</sub>OCH<sub>2</sub>CH<sub>2</sub>O−), 3.89 (AB, *J* = 16.9 Hz, 2H; −OCH<sub>2</sub>COO*t*Bu), 3.70 (AB, *J* = 16.9 Hz, 2H; −OCH<sub>2</sub>COO*t*Bu), 3.93 (AX, *J* = 13.2 Hz, 4H; ArCH<sub>2</sub>Ar), 3.99 (t, *J* = 8.8 Hz, 4H; −OCH<sub>2</sub>CH<sub>2</sub>OCH<sub>2</sub>CH<sub>2</sub>O−), 4.24 (AX, *J* = 14.8 Hz, 4H; ArCH<sub>2</sub>Ar), 4.30–4.50 (overlapped, 8H), 4.35 (AX, *J* = 13.2 Hz, 4H; ArCH<sub>2</sub>Ar), 4.41 (AX, *J* = 12.8 Hz, 4H; ArCH<sub>2</sub>Ar), 4.44 (AB, *J* = 17.3 Hz, 4H; −OCH<sub>2</sub>COO*t*Bu), 4.63 (AB, *J* = 17.3 Hz, 4H; −OCH<sub>2</sub>COO*t*Bu), 4.93 (brs; <sup>+</sup>NH<sub>3</sub>), 5.25 (AX, *J* = 12.4 Hz, 2H; ArCH<sub>2</sub>Ar), 6.27 (brs, 2H; ArH), 6.70 (brs, 2H; ArH), 7.05 (brs, 2H; ArH), 7.38–7.41 (overlapped, 8H; ArH), 7.48 (s, 4H; ArH<sub>TFPB</sub>−), 7.67 ppm (s, 8H; ArH<sub>TFPB</sub>−); ESI<sup>+</sup> MS: *m/z*: 1690 [*n*BuNH<sub>3</sub>C3]<sup>+</sup>.

**Na<sup>+</sup>C3 complex:** Compound 3 (0.002 g, 1.23 × 10<sup>−3</sup> mmol) was dissolved in CDCl<sub>3</sub> (0.4 mL; 3.0 × 10<sup>−3</sup> M solution). Then, a solution of sodium tetrakis[3,5-bis(trifluoromethyl)phenyl]borate salt in CDCl<sub>3</sub> (1.23 × 10<sup>−3</sup> mmol, 6.1 × 10<sup>−3</sup> M) was added and the mixture was stirred for 15 min at room temperature. Then, the solution was transferred to an NMR tube for 1D and 2D NMR spectra acquisition. <sup>1</sup>H NMR (CDCl<sub>3</sub>, 400 MHz, 298 K):  $\delta$  = 0.95 (s, 9H; −C(CH<sub>3</sub>)<sub>3</sub>), 0.96 (s, 18H; −C(CH<sub>3</sub>)<sub>3</sub>), 1.13 (s, 18H; −C(CH<sub>3</sub>)<sub>3</sub>), 1.38 (s, 18H; −C(CH<sub>3</sub>)<sub>3</sub>), 1.51 (s, 9H, 18H; −OC(CH<sub>3</sub>)<sub>3</sub>), 1.52 (s, 9H, 18H; −OC(CH<sub>3</sub>)<sub>3</sub>), 1.88 (m, 2H; −OCH<sub>2</sub>CH<sub>2</sub>OCH<sub>2</sub>CH<sub>2</sub>O−), 2.34 (m, 2H; −OCH<sub>2</sub>CH<sub>2</sub>OCH<sub>2</sub>CH<sub>2</sub>O−), 2.63 (m, 2H; −OCH<sub>2</sub>CH<sub>2</sub>OCH<sub>2</sub>CH<sub>2</sub>O−), 2.88 (m, 2H; −OCH<sub>2</sub>CH<sub>2</sub>OCH<sub>2</sub>CH<sub>2</sub>O−), 3.32 (AX, *J* = 15.2 Hz, 2H; ArCH<sub>2</sub>Ar), 3.54 (AX, *J* = 14.4 Hz, 4H; ArCH<sub>2</sub>Ar), 3.73 (m, 2H; −OCH<sub>2</sub>CH<sub>2</sub>OCH<sub>2</sub>CH<sub>2</sub>O−), 4.02 (brt, *J* = 8.1 Hz, 2H; −OCH<sub>2</sub>CH<sub>2</sub>OCH<sub>2</sub>CH<sub>2</sub>O−), 4.18–4.31 (overlapped, 4H; −OCH<sub>2</sub>CH<sub>2</sub>OCH<sub>2</sub>CH<sub>2</sub>O−), 4.20 (AX, *J* = 14.4 Hz, 4H; ArCH<sub>2</sub>Ar), 4.31 (s, 4H; −OCH<sub>2</sub>COO*t*Bu), 4.44 (s, 2H; −OCH<sub>2</sub>COO*t*Bu), 4.49 (AX, *J* = 14.4 Hz, 4H; ArCH<sub>2</sub>Ar), 5.09 (AX, *J* = 15.2 Hz, 2H; ArCH<sub>2</sub>Ar), 6.58 (brs, 2H; ArH), 6.96 (brs, 2H; ArH), 7.02 (brs, 2H; ArH), 7.17 (brs, 2H; ArH), 7.20 (brs, 2H; ArH), 7.25 (brs, 2H; ArH), 7.28 (brs, 2H; ArH), 7.48 (s, 4H; ArH<sub>TFPB</sub>−), 7.67 ppm (s, 8H; ArH<sub>TFPB</sub>−); <sup>13</sup>C NMR (CDCl<sub>3</sub>, 100 MHz, 298 K):  $\delta$  = 28.1 (q, −C(CH<sub>3</sub>)<sub>3</sub>), 28.2 (q, −C(CH<sub>3</sub>)<sub>3</sub>), 28.4 (t, ArCH<sub>2</sub>), 28.5 (t, ArCH<sub>2</sub>), 30.2 (t, ArCH<sub>2</sub>), 31.3 (q, −C(CH<sub>3</sub>)<sub>3</sub>), 31.4 (q, −C(CH<sub>3</sub>)<sub>3</sub>), 31.7 (q, −C(CH<sub>3</sub>)<sub>3</sub>), 32.2 (t, ArCH<sub>2</sub>), 34.3 (s, −C(CH<sub>3</sub>)<sub>3</sub>), 4C), 34.5 (s, −C(CH<sub>3</sub>)<sub>3</sub>), 6C), 70.1, 70.6, 71.1, 71.3, 73.6, 74.0 (t, OCH<sub>2</sub>), 84.5, 84.6 (s, OC(CH<sub>3</sub>)<sub>3</sub>), 117.6 (d, C<sub>Ar</sub>H<sup>TFPB</sup>), 123.8 (d, C<sub>Ar</sub>H), 125.4 (d, C<sub>Ar</sub>H), 125.5 (d, C<sub>Ar</sub>H), 126.2 (d, C<sub>Ar</sub>H), 126.9 (d, C<sub>Ar</sub>H), 128.6 (d, C<sub>Ar</sub>H), 128.8 (d, C<sub>Ar</sub>H), 135.1 (d, C<sub>Ar</sub>H<sup>TFPB</sup>), 130.5 (s, C<sub>Ar</sub>CH<sub>2</sub>), 131.9 (s, C<sub>Ar</sub>CH<sub>2</sub>), 132.2 (s, C<sub>Ar</sub>CH<sub>2</sub>), 132.9 (s, C<sub>Ar</sub>CH<sub>2</sub>), 133.1 (s, C<sub>Ar</sub>CH<sub>2</sub>), 134.2 (s, C<sub>Ar</sub>CH<sub>2</sub>), 134.6 (s, C<sub>Ar</sub>CH<sub>2</sub>), 135.0 (s, C<sub>Ar</sub>CF<sub>3</sub>), 8C), 146.4 (s, C<sub>Ar</sub>C(CH<sub>3</sub>)<sub>3</sub>), 147.2 (s, C<sub>Ar</sub>C(CH<sub>3</sub>)<sub>3</sub>), 148.1 (s, C<sub>Ar</sub>C(CH<sub>3</sub>)<sub>3</sub>), 148.6 (s, C<sub>Ar</sub>C(CH<sub>3</sub>)<sub>3</sub>), 149.3 (s, C<sub>Ar</sub>O), 150.7 (s, C<sub>Ar</sub>O), 151.9 (s, C<sub>Ar</sub>O), 153.7 (s, C<sub>Ar</sub>O), 170.5 ppm (s, C = O, 3C); ESI<sup>+</sup> MS: *m/z*: 1639 [NaC3]<sup>+</sup>.

**Determination of association constant values by quantitative <sup>1</sup>H NMR spectroscopy analysis:** The samples were prepared by dissolving 3 (1.24 × 10<sup>−3</sup> mmol) and the appropriate alkylammonium guest 5a–d (1.24 × 10<sup>−3</sup> mmol) in CDCl<sub>3</sub> (0.5 mL) containing toluene (1 μL; *d* = 0.87 g mL<sup>−1</sup>, 0.19 M) as an internal standard. The complex concentration was evaluated by integration of the <sup>1</sup>H NMR signals of the toluene CH<sub>3</sub> group versus the shielded signals at negative values of chemical shift of the guest molecules. Equation (1)<sup>[35]</sup> was used to obtain the number of moles of the complex:

$$\frac{G_a}{G_b} = \frac{F_a}{F_b} \times \frac{N_b}{N_a} \times \frac{M_a}{M_b} \quad (1)$$

in which *G<sub>a</sub>* is the number of grams of toluene; *G<sub>b</sub>* is the number of grams of complex; *F<sub>a</sub>* and *F<sub>b</sub>* are the areas of the signals of the toluene

$CH_3$  group and shielded signal of the guest, respectively;  $N_a$  and  $N_b$  are the numbers of nuclei that cause the signals ( $N_a$  for toluene=3;  $N_b$  for the guest); and  $M_a$  and  $M_b$  are the molecular masses of toluene and complex, respectively.

### Acknowledgements

We thank Dr. Patrizia Iannece (Dipartimento di Chimica, Università di Salerno) for ESI-MS measurements.

- [1] For comprehensive reviews on calixarene macrocycles, see: a) C. D. Gutsche, *Calixarenes—An Introduction*, 2nd ed., The Royal Society of Chemistry, Cambridge, **2008**; b) V. Böhmer, *Angew. Chem.* **1995**, *107*, 785–818; *Angew. Chem. Int. Ed. Engl.* **1995**, *34*, 713–745; c) A. Ikeda, S. Shinkai, *Chem. Rev.* **1997**, *97*, 1713–1734.
- [2] a) *Calixarenes 2001* (Eds.: Z. Asfari, V. Böhmer, J. Harrowfield, J. Vicens), Kluwer, Dordrecht, **2001**; b) *Calixarenes in the Nanoworld* (Eds.: J. Vicens, J. Harrowfield), Springer, Dordrecht, **2006**.
- [3] For general accounts see ref. [1], whereas for recent examples of chemical modification of calixarene macrocycle for functionalization to bridging methylenes, see: a) I. Columbus, S. E. Biali, *Org. Lett.* **2007**, *9*, 2927–2929; b) K. Kogan, S. E. Biali, *Org. Lett.* **2007**, *9*, 2393–2396; c) L. Kuno, S. Noa, S. E. Biali, *Org. Lett.* **2007**, *9*, 1577–1580; for the introduction of oxygenated functions into the calix walls, see: d) C. Gaeta, F. Troisi, M. Martino, E. Gavuzzo, P. Neri, *Org. Lett.* **2004**, *6*, 3027–3030; e) F. Troisi, L. Mogavero, C. Gaeta, E. Gavuzzo, P. Neri, *Org. Lett.* **2007**, *9*, 915–918; f) F. Troisi, L. Citro, C. Gaeta, E. Gavuzzo, P. Neri, *Org. Lett.* **2008**, *10*, 1393–1396; g) C. Gaeta, F. Troisi, E. Gavuzzo, M. Camalli, G. Campi, P. Neri, *CrystEngComm* **2010**, *12*, 880–887; h) C. Gaeta, F. Troisi, R. Spagna, M. Camalli, G. Campi, P. Neri, *CrystEngComm* **2011**, *13*, 467–473; a novel approach to functionalize the calixarene *exo* rim with nucleophiles using calixarene *p*-bromodienone derivatives has been recently reported: i) F. Troisi, T. Pierro, C. Gaeta, P. Neri, *Org. Lett.* **2009**, *11*, 697–700; j) F. Troisi, T. Pierro, M. Carratù, C. Gaeta, P. Neri, *Tetrahedron Lett.* **2009**, *50*, 4416–4419; k) C. Gaeta, M. Martino, P. Neri, *Tetrahedron Lett.* **2003**, *44*, 9155–9159; for an analogous procedure in which alkoxy groups are introduced into the calixarene *exo* rim, starting from calixarene spirodienone derivatives, see: l) S. Thulasi, G. V. Bhagavathy, J. Eliyan, L. R. Varma, *Tetrahedron Lett.* **2009**, *50*, 770–772.
- [4] a) A. Arduini, A. Pochini, A. Secchi, F. Ugozzoli in *Calixarenes 2001* (Eds.: Z. Asfari, V. Böhmer, J. Harrowfield, J. Vicens), Kluwer, Dordrecht, **2001**, pp. 457–475, for recent examples, see: b) S. Le Gac, M. Luhmer, O. Reinaud, I. Jabin, *Tetrahedron* **2007**, *63*, 10721–10730; c) D. Coquière, J. Marrot, O. Reinaud, *Org. Biomol. Chem.* **2008**, *6*, 3930–3934; d) D. Coquière, S. Le Gac, U. Darbost, O. Sénèque, I. Jabin, O. Reinaud, *Org. Biomol. Chem.* **2009**, *7*, 2485–2500; e) C. Monnereau, J.-N. Rebilly, O. Reinaud, *Eur. J. Org. Chem.* **2011**, 166–175.
- [5] a) S. E. Matthews, P. D. Beer in *Calixarenes 2001* (Eds.: Z. Asfari, V. Böhmer, J. Harrowfield, J. Vicens), Kluwer, Dordrecht, **2001**, pp. 421–439; for recent examples, see: b) F. Troisi, A. Russo, C. Gaeta, G. Bifulco, P. Neri, *Tetrahedron Lett.* **2007**, *48*, 7986–7989; c) F. Troisi, C. Gaeta, T. Pierro, P. Neri, *Tetrahedron Lett.* **2009**, *50*, 5113–5115; d) T. Pinter, S. Jana, R. J. M. Courtemanche, F. Hof, *J. Org. Chem.* **2011**, *76*, 3733–3741.
- [6] For recent examples, see: a) L. Gregoli, L. Russo, I. Stefio, C. Gaeta, F. Arnaud-Neu, V. Hubscher-Bruder, P. Khazaali-Parsa, C. Geraci, P. Neri, *Tetrahedron Lett.* **2004**, *45*, 6277–6281; b) E. Wani-gasekara, C. Gaeta, P. Neri, D. M. Rudkevich, *Org. Lett.* **2008**, *10*, 1263–1266; c) T. Pierro, C. Gaeta, F. Troisi, P. Neri, *Tetrahedron Lett.* **2009**, *50*, 350–353; d) T. Pierro, C. Gaeta, P. Neri, *Supramol. Chem.* **2010**, *22*, 726–736; e) S. Moerkerke, M. Ménand, I. Jabin, *Chem. Eur. J.* **2010**, *16*, 11712–11719.
- [7] For a review on the chemistry of calix[7]arenes, see: M. Martino, P. Neri, *Mini-Rev. Org. Chem.* **2004**, *1*, 219–231.
- [8] M. Martino, L. Gregoli, C. Gaeta, P. Neri, *Org. Lett.* **2002**, *4*, 1531–1534.
- [9] M. Martino, C. Gaeta, L. Gregoli, P. Neri, *Tetrahedron Lett.* **2002**, *43*, 9521–9525.
- [10] M. Martino, C. Gaeta, P. Neri, *Tetrahedron Lett.* **2004**, *45*, 3387–3391.
- [11] Z. Luo, S. Gong, C. Zhang, Q. Zheng, Y. Chen, *Synlett* **2006**, *5*, 795–797.
- [12] H. Li, D. Xiong, Y. Chen, P. Xie, J. Wan, *J. Inclusion Phenom. Macrocyclic Chem.* **2008**, *60*, 169–172.
- [13] C. Gaeta, T. Caruso, M. Mincoletti, F. Troisi, E. Vasca, P. Neri, *Tetrahedron* **2008**, *64*, 5370–5378.
- [14] L. Erra, C. Tedesco, G. Vaughan, M. Brunelli, F. Troisi, C. Gaeta, P. Neri, *CrystEngComm* **2010**, *12*, 3463–3466.
- [15] a) C. Gaeta, F. Troisi, P. Neri, *Org. Lett.* **2010**, *12*, 2092–2095; b) C. Talotta, C. Gaeta, T. Pierro, P. Neri, *Org. Lett.* **2011**, *13*, 2098–2101; c) T. Pierro, C. Gaeta, C. Talotta, A. Casapullo, P. Neri, *Org. Lett.* **2011**, *13*, 2650–2653.
- [16] a) S. H. Strauss, *Chem. Rev.* **1993**, *93*, 927–942; b) H. Nishida, N. Takada, M. Yoshimura, T. Sonoda, H. Kobayashi, *Bull. Chem. Soc. Jpn.* **1984**, *57*, 2600–2604; for recent examples on the use of TFPB superweak anion in supramolecular chemistry, see: c) B. A. Blight, A. Camara-Campos, S. Djurdjevic, M. Kaller, D. A. Leigh, F. M. McMillan, H. McNab, A. M. Slawin, *J. Am. Chem. Soc.* **2009**, *131*, 14116–14122; d) H. Hou, K. C.-F. Leung, D. Lanari, A. Nelson, J. F. Stoddart, R. H. Grubbs, *J. Am. Chem. Soc.* **2006**, *128*, 15358–15359; for a review on counterion effects in supramolecular chemistry, see: e) T. B. Gasca, C. Valente, J. F. Stoddart, *Chem. Soc. Rev.* **2011**, *40*, 57–78.
- [17] a) F. Cunsolo, M. Piattelli, P. Neri, *J. Chem. Soc. Chem. Commun.* **1994**, 1917–1918; b) F. Cunsolo, G. M. L. Consoli, M. Piattelli, P. Neri, *Tetrahedron Lett.* **1996**, 37915–918; c) C. Geraci, M. Piattelli, G. Chessari, P. Neri, *J. Org. Chem.* **2000**, *65*, 5143–5151.
- [18] C. Gaeta, M. Martino, L. Gregoli, P. Neri, *Tetrahedron Lett.* **2002**, *43*, 8875–8878.
- [19] T. Harada, S. Shinkai, *J. Chem. Soc. Perkin Trans. 2* **1995**, 2231.
- [20] a) C. Geraci, G. Chessari, M. Piattelli, P. Neri, *Chem. Commun.* **1997**, 921–922; b) G. M. L. Consoli, F. Cunsolo, C. Geraci, E. Gavuzzo, P. Neri, *Org. Lett.* **2002**, *4*, 2649–2652.
- [21] P. Neri, G. M. L. Consoli, F. Cunsolo, C. Geraci, M. Piattelli in *Calixarenes 2001* (Eds.: Z. Asfari, V. Böhmer, J. Harrowfield, J. Vicens), Kluwer, Dordrecht, **2001**, *5*, pp. 89–109.
- [22] a) G. D. Andreotti, F. Ugozzoli, Y. Nakamoto, S.-I. Ishida, *J. Inclusion Phenom. Mol. Recognit. Chem.* **1991**, *10*, 241–253; b) M. Perrin, S. Lecocq, Z. Asfari, *C. R. Acad. Sci. Ser. 2* **1990**, *310*, 515–520; c) P. Thuéry, M. Nierlich, M. I. Ogden, J. M. Harrowfield, *Supramol. Chem.* **1998**, *9*, 297–303; d) P. Thuéry, M. Nierlich, B. Souley, Z. Asfari, J. Vicens, *J. Chem. Soc. Dalton Trans.* **1999**, 2589–2594; e) J. L. Atwood, M. J. Hardie, C. L. Raston, C. A. Sandoval, *Org. Lett.* **1999**, *1*, 1523–1526; f) R. Ludwig, D. Lentz, T. K. D. Nguyen, *Radiochim. Acta* **2000**, *88*, 335–343.
- [23] a) G. Bifulco, L. Gomez-Paloma, R. Riccio, C. Gaeta, F. Troisi, P. Neri, *Org. Lett.* **2005**, *7*, 5757–5760; b) G. Bifulco, R. Riccio, C. Gaeta, P. Neri, *Chem. Eur. J.* **2007**, *13*, 7185–7194.
- [24] Alternatively, the map superimposition can be done manually by printing the contour plots on transparencies, which can then be overlaid.
- [25] a) C. D. Gutsche, *Calixarenes*, Royal Society of Chemistry, Cambridge, **1989**, pp. 110–111; b) S. Kanamathareddy, C. D. Gutsche, *J. Org. Chem.* **1992**, *57*, 3160–3166; c) C. Jaime, J. de Mendoza, P. Prados, P. M. Nieto, C. Sanchez, *J. Org. Chem.* **1991**, *56*, 3372–3376; d) J. O. Magrans, J. de Mendoza, M. Pons, P. Prados, *J. Org. Chem.* **1997**, *62*, 4518–4520.
- [26] K. B. Lipkowitz, G. Pearl, *J. Org. Chem.* **1993**, *58*, 6729–6736.
- [27] Molecular modeling was performed with the MacroModel-9.0/Maestro-4.1 program: F. Mohamadi, N. G. Richards, W. C. Guida, R. Lis-

- kamp, M. Lipton, C. Caufield, G. Chang, T. Hendrickson, W. C. Still, *J. Comput. Chem.* **1990**, *11*, 440–467.
- [28] F. Ugozzoli, G. D. Andreetti, *J. Inclusion Phenom. Mol. Recognit. Chem.* **1992**, *13*, 337–348.
- [29] K. Hirose, in *Analytical Methods in Supramolecular Chemistry* (Ed.: C. A. Schalley), Wiley-VCH, Weinheim, **2007**, pp. 17–54.
- [30] Y. Tanaka, Y. Kato, Y. Aoyama, *J. Am. Chem. Soc.* **1990**, *112*, 2807–2808.
- [31] F. Arnaud-Neu, S. Fuangwasdi, A. Notti, S. Pappalardo, M. F. Parisi, *Angew. Chem.* **1998**, *110*, 120–122; *Angew. Chem. Int. Ed. Engl.* **1998**, *37*, 112–114.
- [32] Compound **1** was prepared according to the acid-catalyzed one-pot procedure described in: D. R. Stewart, C. D. Gutsche, *J. Am. Chem. Soc.* **1999**, *121*, 4136–4146.
- [33] M. Colapietro, G. Cappuccio, C. Marciante, A. Pifferi, R. Spagna, J. R. Helliwell, *J. Appl. Crystallogr.* **1992**, *25*, 192–194.
- [34] M. C. Burla, R. Caliendo, M. Camalli, B. Carrozzini, G. L. Cascarano, L. De Caro, C. Giacovazzo, G. Polidori, D. Siliqi, R. Spagna, *J. Appl. Crystallogr.* **2007**, *40*, 609–613.
- [35] S. Braun, H.-O. Kalinowsky, S. Berger, *150 and More Basic NMR Experiments: A Practical Course*, Wiley-VCH, Weinheim, **1996**, pp. 232–233.

Received: July 15, 2011  
Published online: December 16, 2011